Acta Pharmaceutica Sinica B 2025;15(2):1126−1142

Chinese Pharmaceutical Association
Institute of Materia Medica, Chinese Academy of Medical Sciences

Acta Pharmaceutica Sinica B

www.elsevier.com/locate/apsb
www.sciencedirect.com

ORIGINAL ARTICLE

Topical adhesive spatio-temporal nanosystem co-delivering chlorin e6 and HMGB1 inhibitor glycyrrhizic acid for *in situ* psoriasis chemo-phototherapy

Lijun Su[a], Yixi Zhu[a], Xuebo Li[a], Di Wang[a], Xiangyu Chen[a], Zhen Liu[a], Jingjing Li[b,*], Chen Zhang[a,*], Jinming Zhang[a,*]

[a]*State Key Laboratory of Southwestern Chinese Medicine Resources, School of Pharmacy, Chengdu University of Traditional Chinese Medicine, Chengdu 611137, China*
[b]*Department of Rehabilitation Sciences, Faculty of Health and Social Sciences, Hong Kong Polytechnic University, Hong Kong SAR 100872, China*

Received 15 August 2024; received in revised form 20 October 2024; accepted 15 November 2024

KEY WORDS

Psoriasis;
Chitosan;
Catechol;
Spatio-temporal nanosystem;
Glycyrrhizic acid liposome;
Chemo-phototherapy;
Topical delivery;
Anti-inflammation

Abstract Recently, photodynamic therapy (PDT) has gained considerable attention as a promising therapeutic approach for the treatment of psoriasis. Unfortunately, the activation of high mobility group box 1 protein (HMGB1) by PDT triggers innate and adaptive immune responses, which exacerbate skin inflammation. Herein, we combined glycyrrhizic acid (GA), a natural anti-inflammatory compound and immunomodulator derived from the herb *Glycyrrhiza uralensis* Fisch., with PDT actuated by the photosensitizer chlorin e6 (Ce6) by co-loading them in GA-based lipid nanoparticles coated with a catechol-modified quaternary chitosan salt (GC NPs/QCS-C). GC NPs/QCS-C exhibited high drug loading efficacy, uniform size distribution, an ideal topical adhesive property, enhanced skin retention and penetration in psoriasis-like lesions, and high intracellular uptake in epidermal cells compared with the counterparts. Subsequently, the transdermal administration of GC NPs/QCS-C followed by near-infrared laser radiation in an imiquimod-induced psoriasis-like mouse model significantly ameliorated psoriasis symptoms, promoted the apoptosis of hyperproliferative epidermal cells, and alleviated the inflammatory cascade. The significant therapeutic outcomes of GC NPs/QCS-C were attributed to the synergistic effects of GA and PDT on modulating immune cell recruitment and inhibiting dendritic cell maturation. Our results demonstrated that the topical bio-adhesive nanosystem that combines GA and Ce6 offers a synergistic chemo-phototherapeutic strategy for psoriasis treatment.

*Corresponding authors.
E-mail addresses: kim07.li@polyu.edu.hk (Jingjing Li), chenzhang_1990@126.com (Chen Zhang), cdutcmzjm@126.com (Jinming Zhang).
Peer review under the responsibility of Chinese Pharmaceutical Association and Institute of Materia Medica, Chinese Academy of Medical Sciences.

https://doi.org/10.1016/j.apsb.2024.12.020

1. Introduction

Psoriasis is a chronic autoimmune-mediated inflammatory dermatosis that is estimated to affect 2%−3% of the global population[1,2]. Due to its complex pathogenesis, conventional treatments using immune inhibitors and newly developed biological agents have failed to achieve satisfactory therapeutic outcomes, as indicated by the high incidence of their side effects and short-term symptomatic relief they afford[3]. Currently, photodynamic therapy (PDT), an emerging approach with minimal invasiveness, low toxicity, and low drug resistance, has been widely used to ameliorate inflammatory dermatoses (*e.g.*, severe acne, rosacea, and psoriasis)[4]. 5-Aminoleavulinic acid (5-ALA)-based PDT has been approved by US. Food and Drug Administration (FDA) as a well-known treatment approach for non-hypertrophic actinic keratoses and superficial basal-cell carcinomas[5]. Its therapeutic advantages are probably attributable to the promotion of inflammatory cell apoptosis and necrosis in the skin by the generation of excessive reactive oxygen species (ROS), which inhibit the proliferation and keratinization of keratinocytes in psoriasis development[6,7]. However, only intracellular 5-ALA that is metabolized into protoporphyrin IX can generate excessive ROS[8]. The therapeutic benefit of 5-ALA is greatly limited by its poor penetration into the thick stratum corneum of psoriatic skin and its poor intracellular accumulation. In comparison, the second-generation photosensitizer chlorin e6 (Ce6) exhibits a higher yield of single-linear oxygen. Ce6-based PDT has been widely used to treat inflammatory diseases and tumors[9,10]. Therefore, the powerful photodynamic effect induced by Ce6 offers a promising treatment approach for psoriasis.

However, PDT not only results in ROS-induced cell death but also triggers the cascade of immunogenic cell death and activates the expression of high mobility group box 1 (HMGB1) protein[11,12]. The activation of HMGB1, in turn, promotes dendritic cell (DC) maturation and accelerates antigen presentation[13], initiating a series of cellular reactions and ultimately activating innate and adaptive immune responses[14]. Although this can potentially be a greatly useful collateral benefit in tumor therapy, it impedes the remission of skin inflammation in psoriasis. We hypothesized that the combination of an HMGB1 inhibitor with PDT would enhance psoriasis treatment outcomes and suppress the downstream inflammatory cascade. Glycyrrhizic acid (GA), a bioactive compound in the herbal medicine *Glycyrrhiza uralensis* Fisch., exhibits promising anti-inflammatory and immunosuppressive potential for the treatment of various diseases. GA is acknowledged as an effective intracellular inhibitor of HMGB1[15,16], possibly interfering with the HMGB1−DNA complex structure[17]. The suppression of HMGB1 by GA has been applied to treat nasal inflammation, ischemic stroke, hepatic inflammation, and vascular endothelial inflammation[18-20]. Therefore, we attempted to enhance the psoriasis remission effect of PDT by combining it with GA, which presents the advantages of inherent anti-inflammatory activity and HMGB1 blockade[21,22].

However, the efficient delivery of GA and Ce6 into psoriasis lesions is a major challenge that remains to be addressed. Compared with oral or intravenous administration, topical treatment for psoriasis is associated with better patient compliance and fewer side effects[23]. Currently, lipid-based nanovehicles are widely recognized as promising carriers for dermal drug delivery due to their effective transdermal penetration and good biocompatibility[24,25]. Their lipidic nature is beneficial to facilitate skin permeation and increase payload bioavailability[26]. In a previous study, by replacing cholesterol with GA, we successfully fabricated a novel GA-based lipid nanovehicle with high lipid membrane stability and drug-loading capacity[27]. Furthermore, when Ce6 was encapsulated in this GA-lipid nanovehicle, the generated spatiotemporal co-delivery nanosystem not only avoided the potential drug−drug interactions between co-delivery agents and the unstable drug ratio in nanoparticles (NPs) but also exhibited compatibility between the lipid membrane and the epidermis.

Furthermore, given the thickness of the cuticle, long-term drug retention and effective drug penetration in the skin remain major challenges in the topical drug delivery system for psoriasis treatment. Chitosan (CS) has been widely used for dermal applications[28], such as to treat burns, wounds, and plaque psoriasis[29-31]. CS-based formulations were recommended to prolong drug retention in the skin and to enhance drug penetration to promote drug diffusion *via* the transcellular or paracellular route[32]. Apart from its well-known antibacterial activity, the strong bioadhesive effect of CS, due to the interaction between its cationic nature and the polyanionic nature of epidermal cells, is a great advantage. However, the poor water solubility of CS greatly limits its application. In comparison, the introduction of quaternary ammonium moieties can provide an effective approach to enhance the positive charge, water solubility, mucoadhesive capacity, cellular uptake, and skin permeability properties of topical drug delivery systems[33].

As a proof of concept, we developed a novel bioadhesive chemo-photodynamic nanosystem for psoriasis treatment, which takes full advantage of the suppression of epidermal cell hyperplasia induced by PDT and falling off the potential PDT-induced inflammatory cascade by the use of GA. Meanwhile, inspired by the catechol-chemistry-based humid adhesive dressing, we fabricated a catechol-modified quaternary chitosan salt (QCS-C) and coated it on GA-based lipid NPs. As shown in the scheme, GC NPs/QCS-C with a shell−core structure were flexibly fabricated. Due to the strong adhesive character of the QCS-C layer, the GC NPs containing GA and Ce6 exhibited enhanced retention and permeation in the thickened skin lesion. Under laser irradiation, the intracellular GC NPs, combined with GA-induced HMGB1 downregulation, induced the apoptosis of abnormal hyperplastic epidermal cells and suppressed the inflammatory cascade (Scheme 1). Potent anti-psoriatic effects of GC NPs/QCS-C were observed in an imiquimod (IMQ)-induced psoriasis mouse model *in vivo*. To the best of our knowledge, this study is the first to develop a flexible topical chemo-phototherapy nanosystem that combines a natural HMGB1 inhibitor and PDT for psoriasis treatment.

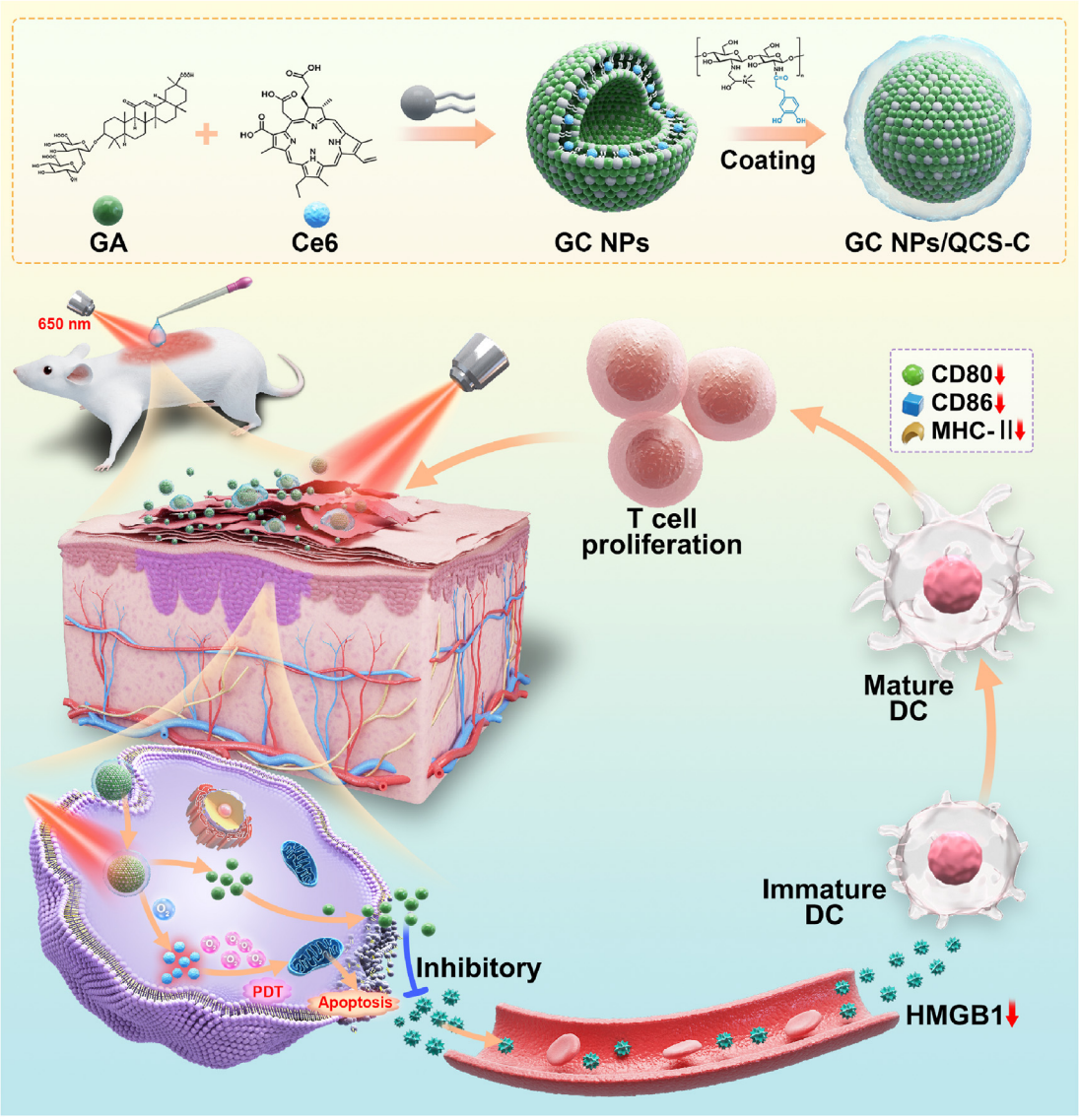

Scheme 1 A novel bioadhesive chemo-photodynamic nanosystem was developed for psoriasis treatment, combing epidermal cell hyperplasia suppression by photodynamic therapy with alleviating the potential induced inflammatory cascade by glycyrrhizic acid.

2. Materials and methods

2.1. Materials

Quaternized chitosan salt (QCS) was purchased from Shanghai Macklin Biochemical Co., Ltd. (Shanghai, China). Glycyrrhizic acid (GA) was purchased from Meilunbio Biotechnology Co., Ltd. (Dalian, China). Chlorin e6 (Ce6) was obtained from Zhengzhou Feynman Biotechnology Co., Ltd. (Zhengzhou, China). Egg yolk lecithin (phosphatidylcholine >68%, phosphatidylethanolamine <20%) was purchased from AVT (Shanghai) Pharmaceutical Tech Co., Ltd. (Shanghai, China). Cell culture medium and fetal bovine serum (FBS) were obtained from Invitrogen (Carlsbad, CA, USA). Imiquimod ointment (5%) was purchased from Zhuhai United Laboratories Co., Ltd. China Mouse HMGB1 ELISA Kit was obtained from Elabscience® Biotechnology Co., Ltd. (Wuhan China). Mouse IL-18 ELISA Kit was obtained from Hangzhou Lianke Biotechnology Co., Ltd. (Hangzhou, China). Dihydroethidium (DHE) was obtained from Uelandy Biotechnology Co., Ltd. (US EVERBRIGHT, Suzhou, China). Annexin V-FITC/PI apoptosis kit was supplied by Beyotime biotechnology (Shanghai, China). Immunohistochemical antibodies of HMGB1, Ki67, CD3, and IL-17 were purchased from Wuhan Servicebio Technology Co., Ltd. (Wuhan, China). Flow Cytometry Antibodies CD3, CD4, CD8, MHC II, CD86 and CD80 were obtained from Biolegend (Biolegend, CA, USA).

2.2. Cell culture and animal feeding

Human Keratinocytes (HaCaT Cells) line purchased from Boster Biological Technology Co., Ltd. (California, US) and cultured in Dulbecco's modified Eagle's medium (DMEM) supplemented with 10% FBS, penicillin (100 U/mL), and streptomycin (100 μg/mL). Male ICR mice, 8 weeks old, weighing 18−20 g, were acquired from SPF Biotechnology Co., Ltd. (Beijing, China), and were housed at 25 °C with a 12-h light−dark cycle. All animal experiments were conducted in accordance with the National Institutes of Health (NIH) Guidelines for the Care

and Use of Laboratory Animals and the Guidelines for the Care and Use of Laboratory Animals approved by the Ethics Committee of the School of Pharmacy, Chengdu University of Traditional Chinese Medicine (Certificate of Ethical Review for Laboratory Animal Welfare No. 2024013).

2.3. Synthesis of catechol-modified quaternized chitosan salt (QCS-C)

QCS-C was synthesized based on previous references[34-37]. Specifically, 25 mL of anhydrous ethanol containing 1 g catechol and 1.15 g EDC-HCl (Macklin) was added dropwise to 100 mL QCS solution (0.01 g/mL). Adding 0.69 g NHS (Macklin) as a catalyst, the mixture was stirred at 25 °C for 24 h. The purified QCS-C was then obtained by dialysis method (MWCO: 3500 Da) for 3 days against deionized water and then freeze-dried. The QCS-C grafts were characterized using FT-IR, ^{1}H NMR, and XRD. Specific analytical methods are described in Supporting Information

2.4. Preparation of Ce6-loaded GA-lipid NPs coated by QCS-C (GC NPs/QCS-C)

GC NPs/QCS-C were prepared by two-step method. Primarily, the Ce6-loaded GA-lipid NPs were obtained *via* the combined ethanol injection and ultrasonic emulsification method. Briefly, 6 mg of GA, 30 mg of egg yolk lecithin, and 1 mg of Ce6 were accurately weighed and co-dissolved in 2 mL of anhydrous ethanol. The mixture was then slowly dropped into 10 mL of purified water and stirred for 1 h. The liquid suspension was sonicated for 5 min in ice bath with a sequence of 3 s of sonication and 2 s of suspension by an Ultrasonicator (Ymnl-1000Y, Nanjing, China). And then, GC NPs coated with QCS-C were readily prepared by the physical interaction. 1 mg/mL of QCS-C solution was added dropwise into the GC NPs suspension (0.5:10, *v*/*v*), keeping stirring for 30 min and then obtain GC NPs/QCS-C suspension. The unloaded agents and large particles were removed by 0.45 μm microporous membrane ultrafiltration. Similarly, a replacement of GA with cholesterol and then Ce6 NPs/QCS-C was prepared. GC NPs/QCS, GA NPs, and GA NPs/QCS-C were prepared by the same method.

2.5. Characterization of GC NPs/QCS-C

The size distribution and zeta potential of GC NPs/QCS-C were measured using a dynamic light scattering particle size analyzer (Litesizer 500, Anton Paar, Austria). Its morphology was observed by a transmission electron microscope (HT-7800, Ruli TEM, Japan), with the detailed characterization methods listed in Supporting Information

2 mL of GC NPs/QCS-C was dissolved in 10 mL of methanol with ultrasound treatment. The suspension was filtered by 0.22 μm millipore filter. The concentrations of GA and Ce6 in suspension were quantified by high-performance liquid chromatography (HPLC, Ultimate 3000, Thermo Fisher, US). Cosmosil C_{18} column (250 mm × 4.6 mm, 5 μm) was used at 25 °C. The flow rate and injection volume were 1.0 mL/min and 10 μL, respectively. For GA detection, the mobile phase was methanol/0.1% phosphoric acid in water (*v*/*v*) with a volume ratio of 75:25, and the detective wavelength was 250 nm. Additionally, the mobile phase for Ce6 determination was acetonitrile/0.1% phosphoric acid water (*v*/*v*) with a volume ratio of 50:50, and the detective wavelength was 405 nm.

The encapsulation efficiency (EE) and loading efficiency (LE) were calculated[38], based on the following Eqs. (1) and (2):

$$\text{LE}\ (\%) = (\text{Weight of drug in NPs}) / (\text{Weight of NPs}) \times 100 \quad (1)$$

$$\text{EE}\ (\%) = (\text{Weight of drug in NPs}) / (\text{Weight of added drug}) \times 100 \quad (2)$$

The storage stability of GC NPs/QCS-C suspension was examined by measuring the changes of particle size and zeta potential, for 30 consecutive days at 4 °C. Meanwhile, the photostability of GC NPs/QCS-C during a 15-day storage period was also evaluated by the changes of particle size, LE and EE of payloads.

The viscosities of GC NPs, GC NPs/QCS and GC NPs/QCS-C suspensions were tested with a rotational rheometer (MCR 102e, Anton Paar)[39]. Suspensions were taken at room temperature 25 °C temperature in a certain direction to gradually increase the shear rate (0.1−100 1/S) to test the relationship of suspension viscosity with shear rate.

2.6. Drug release from GC NPs/QCS-C

The *in vitro* drug release profile of GC NPs/QCS-C was evaluated by dialysis bag method. Briefly, 2 mL of GC NPs/QCS-C suspension freshly prepared was placed in a dialysis bag (MWCO: 1000 Da) against 30 mL PBS containing 0.1% (*w*/*v*) Tween 80 (pH 7.4) under continuous shaking (80 rpm) at 37 °C. At predetermined time points (0, 0.5, 2, 4, 6, 8, 12, 24 h), 1 mL of release medium was drawn out and replenished with an equal volume of fresh dialysis medium. These collected samples were mixed with the equivolumetric methanol and then filtrated through a 0.22 μm membrane filter. The amounts of GA and Ce6 were detected by HPLC (Thermo Fisher) based on the aforementioned methods. Likewise, the release profiles of free GA, free Ce6, and GC NPs were also implemented.

2.7. In vitro singlet oxygen generation

The production capacity of singlet oxygen derived from GC NPs/QCS-C under laser irradiation was detected by singlet oxygen sensor green fluorescent probe (SOSG) (Meilunbio Dalian, China). Briefly, 50 μL of SOSG (25 μmol/L) was added to 1 mL of free Ce6, and GC NPs/QCS-C, in which the Ce6 concentration was equivalently 100 μg/mL, respectively. The amounts of singlet oxygen generated in these samples were detected under laser irradiation (650 nm, 0.5 W/cm^2) for different periods. The fluorescence signal intensity was measured by fluorescence spectrophotometer (Guangdong F-380, China). As a negative control, the samples without irradiation treatment were used.

2.8. Cellular uptake in vitro

HaCaT cells were seeded into 6-well plates (2×10^5 cells/mL) and incubated at 37 °C overnight for cell adherence. After then, fresh culture medium containing free Ce6, GC NPs, and GC NPs/QCS-C (Ce6 equivalent concentration of 30 μg/mL) were respectively added and incubated for 2 h. Then, the cells were rinsed with cold PBS for 3 times. After fixing in paraformaldehyde for 15 min, the cell nuclei and cytoskeleton were stained with DAPI (Beyotime Biotech Co., Ltd., China) and

phalloidin (Biosharp, China). Finally, cells were imaged using a laser confocal microscope (CLSM, TSC SP8, Leica, Germany). The excitation and emission wavelength (Ex/Em) for DAPI, phalloidin, and the intracellular Ce6 determination was 364/454 nm, 545/570 nm, and 488/520 nm, respectively.

Additionally, the cellular uptakes of GC NPs/QCS-C in HaCaT cells were also quantitatively determined by flow cytometer (FCM) (FACS Canto II, Thermo Fisher, US). Similarly, HaCaT cells were seeded into 6-well plates (2×10^5 cells/mL). After cell adherence, cells were cultured with fresh culture medium containing free Ce6, GC NPs, and GC NPs/QCS-C (Ce6 equivalent concentration of 30 μg/mL) for 2 h. Finally, the cells were washed with PBS for twice, and collected into cell suspension in PBS. The intracellular fluorescence of Ce6 in each group was quantified using FCM (Thermo Fisher).

2.9. *In vitro cytotoxicity efficacy*

HaCaT cells were seeded into 96-well plates (5×10^3 cells/well) overnight. After 24 h of culture, HaCaT cells were treated with free Ce6, Ce6 NPs/QCS-C and GC NPs/QCS-C with the same concentration of Ce6 (0.006−6 μg/mL). After 2h of treatment, cells were exposed to laser irradiation (650 nm, 0.5 W/cm^2) for 3 min. After the additional 24 h of incubation, cell cytotoxicity was assessed using CCK-8 assay (Biosharp, China). Likewise, the cytotoxicity of free GA and GA NPs/QCS-C with the GA concentration at 0.05−50 μg/mL was also determined. The percentage of the treated group *versus* the untreated control group was calculated as cell viability.

2.10. *Intracellular ROS measurement and cell apoptosis assays*

HaCaT cells (2.0×10^5 cells/mL) were seeded overnight in 24-well plates. Then, the fresh culture medium containing free GA, GA NPs/QCS-C, free Ce6, Ce6 NPs/QCS-C and GC NPs/QCS-C was added in cell well, in which the concentration of GA and Ce6 was 250 and 30 μg/mL, respectively. After 2 h of incubation, cells treated with these formulations containing Ce6 were exposed to 650 nm, 0.5 W/cm^2 laser irradiation for 3 min. After additional 4 h treatment, the cells were washed twice with cold PBS and stained with DHE dye at the concentration of 50 μmol/mL for 30 min. And then, cells were washed twice with PBS and prepared as cell suspension. The fluorescence intensity derived from the intracellular DHE was quantified using FCM (Thermo Fisher).

Likewise, HaCaT cells were treated with various formulations by the similar above-mentioned approach. After additional 4 h of treatment, the cells were collected and stained by the Annexin V-FITC/PI Apoptosis Detection Kit. The apoptosis rate of each group was analyzed using FCM (Thermo Fisher).

2.11. *Skin retention and penetration of GC NPs/QCS-C in psoriatic mice*

To evaluate the skin retention with rinsing resistance on psoriatic mice, 1 mL of GC NPs/QCS-C was spread evenly on back skin of healthy mice and psoriasis mice, respectively. After 5 min of treatment, the skin was gently washed with PBS. The skin before and after washing was imaged using a multifunctional imaging system (UVP iBox Scientia, Analytik Jena, Germany) to quantify the residual fluorescence.

Similarly, we also investigated the retention and penetration capacity of GC NPs/QCS-C on psoriatic skin, compared to free Ce6, GC NPs, and GC NPs/QCS. After treatment for 2, 24 and 48 h, respectively, the mice were imaged by a multifunctional imaging system. Meanwhile, dorsal skin sections of psoriatic mice were harvested at 2 and 48 h post-treatment. The penetrated fluorescence in skin tissue was imaged by an automatic biological microscope (DM6B, Leica, Germany).

2.12. *In vitro transdermal capacity of GC NPs/QCS-C*

In vitro transdermal delivery ability of GC NPs/QCS-C was carried out on Franz diffusion cells (RYJ-6B, Huanghai drug inspection instrument, Shanghai, China). The dorsal skin of psoriatic mice was immobilized between the recipient chamber and donor chambers. Free GA, free Ce6, GC NPs, and GC NPs/QCS-C suspensions were placed into donor chambers, respectively. Ultrasonically treated receiving medium (8 mL PBS, pH 7.4) was added to the receiving cell. The device was placed in water bath at 37.5 ± 0.5 °C with magnetic stirring at 100 rpm. At the predetermined time points (0, 1, 2, 4, 12, 24, 36, 48 h), 500 μL of the receiving medium was taken, and the same volume of fresh medium was added immediately to keep the volume constant. Concentrations of GA and Ce6 in the receiving samples were determined by HPLC (Thermo Fisher). The cumulative release rates of GA and Ce6 were determined.

2.13. *Chemo-photodynamic treatment of psoriasis in vivo*

After 5 consecutive days of IMQ administration, the mice presented some typical symptoms of psoriasis, like skin erythema and exanthema desquamativum. And then, these modeled mice were randomly divided into Model group without administration, GA NPs group, GA NPs/QCS-C group, Ce6 NPs/QCS-C group, Ce6 NPs/QCS-C NIR group, GC NPs/QCS-C group, and GC NPs/QCS-C NIR group. These mice without IMQ treatment were acted as the untreated control group, 6 mice were in each group. Drugs were administered on two consecutive days beginning on Day 6. Each mouse received 200 μL of drug at a dose of 500 μg/mL for GA and 60 μg/mL for Ce6. 2 h after administration, mice in the irradiation group were irradiated with a 650 nm laser at 0.5 W/cm^2 for 3 min.

All mice were scored and weighed daily. The PASI score was used to assess the severity of the disease, including the degree of erythema, thickness and scaling. Sections were scored independently on a scale of 0−4. The mice were sacrificed on the eighth day. The levels of HMGB1 and IL-18 in serum samples were determined by ELISA kits. The back skin tissues were harvested and fixed with paraformaldehyde. Paraffin-embedded sections were made with hematoxylin and eosin (H&E) staining. The levels of HMGB1, Ki67, CD3, and IL-17 in the skin tissues were detected by immunohistochemistry (IHC). ImageJ software was used to perform the quantitative analysis.

2.14. *Effects of chemo-photodynamic on the immune system*

To determine the effects of chemo-photodynamic therapy of GC NPs/QCS-C on the body immune system, spleen organs were minced and filtered through 70-mm cell sieves to prepare single-cell suspensions. The single-cell suspensions were incubated with anti-mouse CD3, anti-mouse CD4, anti-mouse CD8 antibodies. The cells were then detected using FCM (Thermo Fisher).

To determine the DCs maturation, lesions skin and spleens were minced and passed through 70-mm cell sieves to prepare

single-cell suspensions. The single-cell suspensions were incubated with anti-mouse CD80, anti-mouse CD86, anti-mouse MHC-II antibodies. Similarly, the cell suspension was determined by FCM (Thermo Fisher).

2.15. *Statistical analysis*

Statistical analysis was performed using GraphPad Prism 8.0 software (GraphPad Software, USA). The unpaired Student's *t*-test or one-way ANOVA test was used to determine statistical differences. Data are presented as mean ± standard deviation (SD). Significance is shown on graphs as $*P < 0.05$, $**P < 0.01$, $***P < 0.001$.

3. Results

3.1. *Characterization of QCS-C*

The successful synthesis of QCS-C was confirmed using ^{1}H NMR, FT-IR, and XRD. Dihydrocaffeic acid (CA) was grafted onto the QCS chain by a coupling reaction of EDC and NHS to obtain QCS-C (Fig. 1A). QCS showed characteristic peaks for CS, $\delta = 3.63$ ppm (H3−H6) and $\delta = 3.76$ ppm (H2, GluNAc). In addition, two characteristic peaks at 3.2 and 4.3 ppm for QCS were attributed to the introduction of the GTMAC trismethylammonium and −NH−CH_2− proton, and the characteristic peaks in the range of 6.5−7.5 ppm were attributed to the catechol moiety introduced by protocatechuic acid (Fig. 1B). The CA grafting rate of QCS-C was 11.61% by ^{1}H NMR.

Strong bands were observed in the range of 3200−3500 cm^{-1}. These bands correspond to the N−H and O−H stretching vibrations of CS. Contrary to QCS, CS did not show a band at 1598 cm^{-1} because of the reaction at the −NH_2− site on the QCS chain, where the primary amines were converted to secondary amines. Furthermore, FT-IR analysis of CS showed bands at approximately 1420 and 1320 cm^{-1} (Fig. 1C), while QCS-C showed no bands. The carboxyl group on catechin and the amine group on CS were linked by amination.

The XRD spectra of QCS and GC NPs/QCS-C are presented in Supporting Information Fig. S1. QCS exhibits a broad peak at $2\theta = 20°$, while QCS-C graft displays a characteristic peak at $2\theta = 22°$. The shift in characteristic peaks indicates that the grafting reaction altered the physical structure of QCS. This is primarily due to the incorporation of catechol groups into the QCS skeleton, which disrupted its crystal structure and increased the amorphous phase.

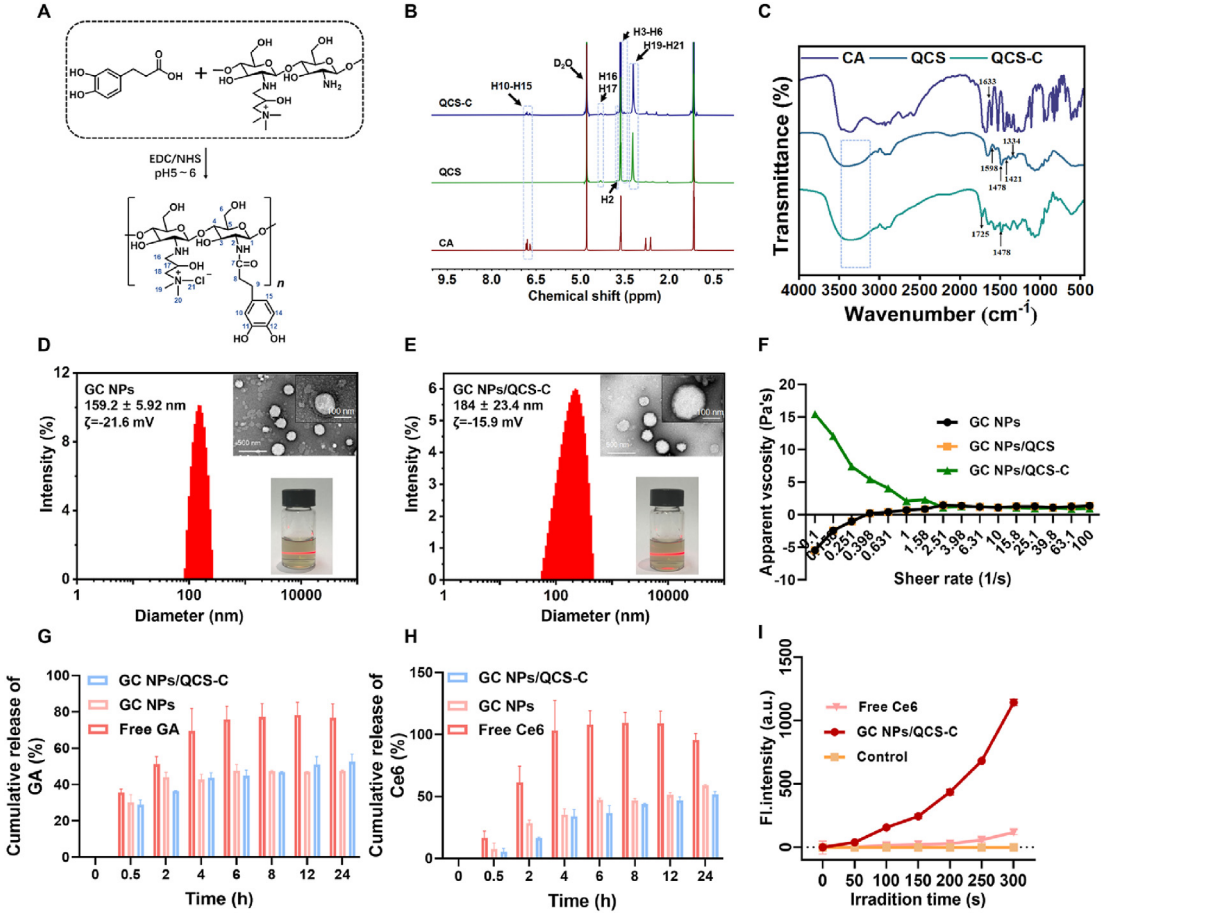

Figure 1 Characterization of GC NPs/QCS-C. (A) Schematic of QCS-C synthesis. (B) ^{1}H NMR spectra of QCS-C, QCS, and CA. (C) FT-IR spectra of CA, QCS and QCS-C. Size distribution and TEM images of GC NPs (D) and GC NPs/QCS-C (E). (F) Apparent viscosity values of GC NPs, GC NPs/QCS, and GC NPs/QCS-C (scale bar = 100 and 500 nm). The *in vitro* release of GA (G) and Ce6 (H) from free GA, free Ce6, GC NPs, and GC NPs/QCS-C *in vitro* release profiles. (I) PDT efficiency of free Ce6, GC NPs/QCS-C based on SOSG probe determination. Data are presented as mean ± SD ($n = 3$).

3.2. Characterization of GC NPs/QCS-C

The morphology and particle distribution of GC NPs and GC NPs/QCS-C are shown in Fig. 1D and E. The average particle sizes of GC NPs and GC NPs/QCS-C measured using DLS were 159.2 ± 5.92 and 184 ± 23.4 nm, respectively. The ζ potentials of GC NPs and GC NPs/QCS-C were −21.6 and −15.9 mV, respectively. The morphology of GC NPs and GC NPs/QCS-C examined by TEM revealed complete spheres with a uniform size. The particles of GC NPs/QCS-C were slightly larger than those of GC NPs, and this difference was attributable to the adsorption and encapsulation of QCS-C on the surface of the liposomes during the preparation process. Similarly, the TEM results clearly showed enhanced shadowing on the surface of GC NPs/QCS-C, further confirming the successful encapsulation of QCS-C onto the liposomal surface. The EE of Ce6 in GC NPs and GC NPs/QCS-C was 80.60% and 90.39%, respectively, while that of GA in GC NPs and GC NPs/QCS-C was 91.39% and 93.48%, respectively. Characterization data (particle size, potential, EE and LE) of GA NPs, GA NPs/QCS-C, Ce6 NPs/QCS-C and GC NPs are displayed in the Supporting Information Fig. S2A and S2B.

During seven days of storage, Ce6 NPs/QCS-C exhibited large fluctuations in particle size potential, and the rest of the liposomes showed better stability (particle size, potential, and encapsulation rate), which further illustrates the stabilizing effect of GA on liposome (Fig. S2C and S2D).

The stability of GC NPs/QCS-C was evaluated by particle size and ζ potential measurement over 30 days at 4 °C under light-protected conditions. After the 30-day storage period, GC NPs/QCS-C demonstrated enhanced stability compared with GC NPs, indicated by the maintenance of a uniform particle size distribution of the former, as shown in Fig. S2E. The QCS-C, which was initially wrapped around the liposomes *via* electrostatic interaction, began to detach from the liposome after 30 days of storage, as indicated by the TEM findings of GC NPs/QCS-C (Fig. S2F). This detachment led to a decrease in the size of GC NPs/QCS-C over the 30-day storage period.

Next, we conducted a photostability evaluation of GC NPs/QCS-C over a 15-day storage period. As shown in Fig. S2G, the particle size of the NPs exhibited uniformity and stability throughout the 15-day storage period, even under non-light-protected conditions, indicating that the light had no discernible impact on the particle size of GC NPs/QCS-C. Additionally, the EE and LE of GA and Ce6 of GC NPs/QCS-C were examined by HPLC. The EE of GA was found to decrease from 86% to 60% and LE from 16% to 10%, while the EE of Ce6 decreased from 98% to 82% and LE from 1.5% to 1.76%. These findings indicate that GC NPs/QCS-C require light protection during storage. Therefore, in the subsequent step, these NPs were formulated into lyophilized powders to ensure optimal light-protected storage.

We expected QCS-C-coated GC NPs to have enhanced skin retention ability. To indirectly substantiate this hypothesis, we employed a rotational rheometer to assess the adhesive properties of the NP suspension before and after polysaccharide encapsulation. The results showed that GC NPs/QCS-C presented a viscosity that gradually decreased with the increase in shear rate, indicating that GC NPs/QCS-C had shear-thinning properties. In contrast, GC NPs did not exhibit shear-thinning characteristics, and their viscosity was not as high as that of GC NPs/QCS-C (Fig. 1F).

The *in vitro* release profiles of GA and Ce6 from GC NPs/QCS-C during the first 24 h was determined. As shown in Fig. 1G and H, both free GA and free Ce6 exhibited rapid release and accumulation. Free GA and free Ce6 are essentially consistent with the drug release first−order equation (Fig. S3A). After 6 h, the cumulative rates of free GA and free Ce6 exceeded 80% and nearly approached 100%. Nevertheless, GC NPs and GC NPs/QCS-C exhibited a sustained release of payloads. After 24 h, less than 50% of the accumulated GA and Ce6 could be released from GC NPs and GC NPs/QCS-C. During that period, due to the structure of GC NPs, GA molecules interacted with lecithin and were distributed on the lipid bilayer, whereas Ce6 was distributed in the interlayer of the lipid bilayer. Therefore, the release rate of GA was slightly higher than that of Ce6 because of their different spatial distribution in GC NPs. These results suggest that the encapsulation of the GC NPs/QCS-C carrier significantly improved the drug release profiles by facilitating controlled release. The Ce6 release from the nanocarriers was determined by dissolving the GC NPs/QCS-C in water and irradiating it with NIR for 10 min. The supernatant was collected, centrifuged at 10,000 rpm for 10 min (TGL-25M, Luxiangyi, China), and the liquid phase was used to determine the supernatant to obtain the cumulative Ce6 release. It can be seen that the NIR treatment triggered the release of Ce6 from the Nano systems, and 90% of Ce6 was released after 10 min of irradiation (Fig. S3B).

The PDT efficiency of GC NPs/QCS-C after laser irradiation was evaluated using an SOSG reactive oxygen probe. Little fluorescence was observed in control groups (Fig. 1I). Free Ce6 could not produce sufficient single-line oxygen, but the fluorescence intensity of GC NPs/QCS-C increased significantly after irradiation. Meanwhile, we also attempted another SOSG fluorescence determination approach with 3 min of continuous irradiation. Fig. S3C shows that after continuous irradiation, the fluorescence intensity of GC NPs/QCS-C was much higher than that of free Ce6. These results indicate that the encapsulation of Ce6 in GC NPs/QCS-C greatly promoted the single-line oxygen production capacity and improved the PDT efficiency.

The low and high doses of free Ce6 and GC NPs/QCS-C both showed an increase in temperature after 10 min of continuous irradiation, and neither the GA NPs/QCS-C nor the water group showed an increase. As shown, after laser irradiation for 10 min, the different temperature changes caused by free Ce6 and GC NPs/QCS-C (Fig. S3D and S3E). The water and GA NPs/QCS-C without Ce6 containing were employed as controls. The photothermal effect of free Ce6 was limited, which only resulted in 9 °C elevation. Nevertheless, high dose of GC NPs/QCS-C could increase 15 °C after 10 min of laser irradiation.

3.3. Enhanced uptake, ROS production, and cell apoptosis in HaCaT cells by GC NPs/QCS-C

We evaluated the blood compatibility of GC NPs, GC NPs/QCS and GC NPs/QCS, and the results showed that all three groups of nanoparticles had good blood compatibility and similar absorbance to the Control group (Fig. S3F). The cellular uptake of free Ce6, GC NPs, and GC NPs/QCS-C NPs by HaCaT cells was assessed both qualitatively and quantitatively using confocal microscopy and flow cytometry, respectively. As depicted in Fig. 2A, after a 2-h incubation period, CLSM revealed a significantly higher level of green fluorescence in the cells treated with NPs than in those treated with free Ce6. This observation suggests that the NPs enhanced the cellular uptake of Ce6. In comparison, cells treated with GC NPs/QCS-C exhibited higher fluorescence intensity than those treated with GC NPs, which may be explained

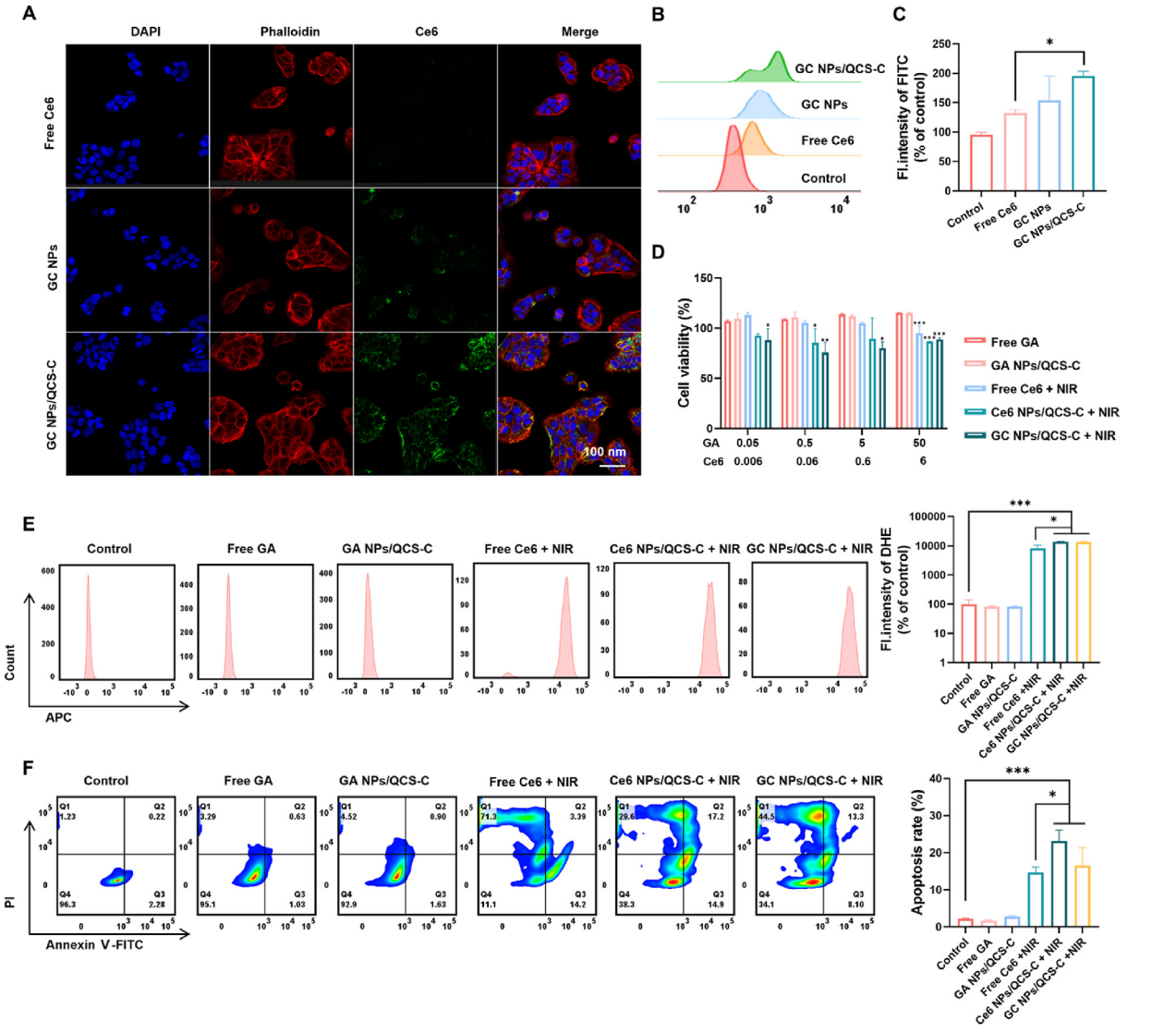

Figure 2 Cellular uptake, cytotoxicity, ROS production, and cell apoptosis induced by GC NPs/QCS-C in HaCaT cells. (A) CLSM images of cellular uptake after 2 h treatment with different Ce6 formulas (scale bar = 100 nm). (B, C) Statistical results of FITC fluorescence of each group by FCM determination. (D) Cell viability against HaCaT cells treated by different formulas at a series of concentrations for 24 h by CCK-8 assay. FCM determination of ROS production (E) and apoptosis rate by Annexin V-FITC double staining. (F) In HaCaT cells after treatment with different formulas NPs for 4 h. Data are presented as mean ± SD ($n = 3$). Note: significance as $^{*}P < 0.05$, $^{***}P < 0.001$.

by the permeation and adhesion effect of the QCS-C coating[40]. Quantitative FCM results (Fig. 2B and C) also corroborated that the uptake of GC NPs/QCS-C in HaCaT cells was greater than that of other NPs.

The cytotoxicity of free GA, free Ce6, GA NPs/QCS-C, Ce6 NPs/QCS-C, and GC NPs/QCS-C to HaCaT cells at a series of concentrations was evaluated using a CCK-8 assay (Fig. 2D). Ce6 NPs/QCS-C were prepared using a similar approach to GC NPs/QCS-C, except that no GA was added to the NPs. The results showed that after 24 h of treatment, none of the GA formulations, including free GA and GA NPs/QCS-C, attenuated cell viability. However, under laser radiation, the Ce6 formulations remarkably reduced cell viability in a concentration-dependent manner, among which GC NPs/QCS-C exerted the strongest cytotoxicity against HaCaT cells at each concentration. This is consistent with the enhanced cellular uptake profiles of GC NPs/QCS-C.

To determine the efficiency of PDT-induced cell death, we examined ROS production in HaCaT cells induced by different formulas using a DHE fluorescent probe. The results showed that neither free GA nor GA NPs/QCS-C without Ce6 loading resulted in ROS production. Nevertheless, treatment with Ce6 formulations significantly increased intracellular ROS accumulation due to the Ce6-induced PDT effect (Fig. 2E). The quantitative result showed that Ce6-loaded NPs including Ce6 NPs/QCS-C and GC NPs/QCS-C had a stronger ability to generate intracellular ROS than free Ce6. Subsequently, the apoptosis activities in HaCaT cells were also evaluated using the Annexin V-FITC double staining method. Similar to the above findings, GA formulations without Ce6 did not induce cell apoptosis, whereas Ce6-loaded NPs greatly promoted the occurrence of apoptosis (Fig. 2F). All of these results indicate that GC NPs/QCS-C were effectively internalized into HaCaT cells, where they generated ROS to promote

apoptosis and cell cytotoxicity, whereas GA formulations demonstrated a high level of biosafety.

3.4. *Enhanced retention and penetration of GC NPs/QCS-C in vivo*

We investigated the waterproofing properties of GC NPs/QCS-C on psoriatic skin by applying them to the dorsal skin of IMQ-induced mice and healthy control mice. The results showed no significant change in fluorescence on the dorsal skin of IMQ-induced mice. Approximately 82% of the fluorescence was retained after rinsing the IMQ-induced mice skin with water. Notably, GC NPs/QCS-C were easily removed from healthy control mice. by rinsing with water and wiping (Fig. 3A and B), and only 40% of the fluorescence was retained. This transient non-bioadhesion of GC NPs/QCS-C to healthy control mice. and limited binding of GC NPs/QCS-C to the superficial layer of the intact normal stratum corneum may explain the observed phenomenon.

A challenge often encountered in *in situ* dermal drug delivery is the limited retention of the medication at the application site. To validate that QCS-C-coated liposomes improved drug retention in psoriatic skin, we applied the same amount of free Ce6, GC NPs, GC NPs/QCS, and GC NPs/QCS-C to IMQ-induced mice and performed imaging at the same time points over 48 h. The results showed that the GC NPs/QCS-C group had higher drug retention with longer action on the skin. At 48 h, the GC NPs/QCS-C group exhibited a higher fluorescence intensity (2×10^4) than the other groups. Additionally, approximately 83% of the fluorescence remained on the back after 48 h (Fig. 3C and D). Skin sections

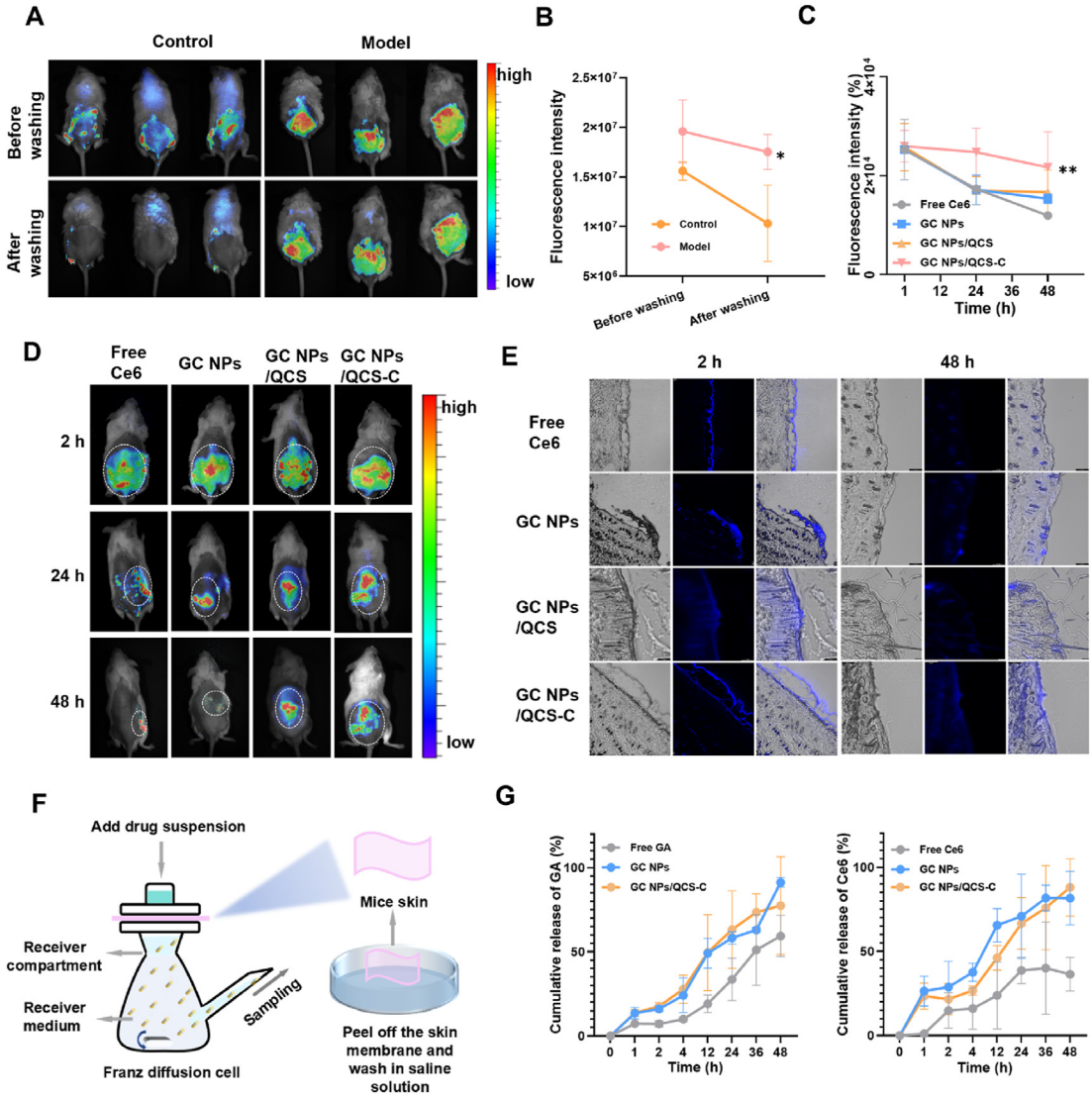

Figure 3 Evaluation of GC NPs/QCS-C adhesion and penetration on psoriatic skin. (A) Spread the GC NPs/QCS-C evenly on dorsal skin of normal and psoriatic mice, with or without rinsing with PBS. (B) Fluorescence intensity quantification of mice dorsal skins with different treatment. (C) Fluorescence intensity of mice dorsal skins after treatment with different formulations at different time-points. (D) Fluorescence imaging of dorsal skin of psoriasis model mice after different time-points. (E) After spreading with GC NPs/QCS-C for 2 and 48 h, mice skin tissues were observed with fluorescence microscope (scale bar = 100 μm). (F) Schematic representation of transdermal drug tests with Franz diffusion cells *in vitro*. (G) *In vitro* transdermal permeation profiles of GA and Ce6 on skin tissues from psoriatic mice over 48 h. Data are presented as mean ± SD ($n = 3$). Note: Significance as $^*P < 0.05$, $^{**}P < 0.01$.

from each group of mice were sampled at 2 h and 48 h and observed for drug penetration and retention. The GC NPs/QCS-C group showed more effective drug retention than the other groups, as evidenced by the higher fluorescence intensity (Fig. 3E). These results suggest that GC NPs/QCS-C can serve as an efficient carrier for drug delivery to psoriatic skin due to their ability to penetrate the skin and form a water-resistant adherence to the tissue during the penetration process.

The transdermal delivery efficiency of GC NPs/QCS-C on the psoriatic skin of mice was investigated using Franz diffusion cells *in vitro*. As shown in Fig. 3F, neither GA nor Ce6 in free drug form could permeate the mouse skin tissue efficiently. The cumulative transdermal drug rate after 48 h was 59.32% and 36.41% for free GA and free Ce6, respectively (Fig. 3G). However, NPs exhibited higher transdermal delivery efficiency than the free drug form. The transdermal cumulative curves of GC NPs and GC NPs/QCS-C were highly similar. The encapsulation of GC NPs/QCS-C promoted the transdermal penetration of payloads, mainly due to the high biocompatibility of liposomes. The lecithin in liposomes has an affinity for the phospholipids present in skin cell membranes, which facilitated the penetration of the liposomal structure through the skin. This result indicates that GC NPs/QCS-C significantly facilitated the penetration of transdermally delivered drugs.

3.5. *In vivo chemo-photodynamic therapy with GC NPs/QCS-C*

The study investigated the efficacy of chemo-photodynamic therapy using an IMQ-stimulated mouse model. Fig. 4A shows the dosing strategy for this experiment, including representative images of the dorsal skin and dorsal blood vessels in different treatment groups on Days 1, 5, and 8. The skin of the model mice showed signs of thickening, erythema, and desquamation. The disease was attenuated, but not significantly so, in the GA-only and PDT-only treatment groups. However, the GA and PDT co-treatment group showed significant reductions in erythema, thickening, and scaling. In addition, as vascular growth in the dermis is a characteristic feature of psoriasis, the dorsal skin was assessed for vascular growth on Day 8. The dorsal blood vessel demonstrated that IMQ had successfully induced psoriasis-like dermatitis. Due to metabolic abnormalities and inflammatory responses, there was significant vascular proliferation and branching in the model group. In addition, the group treated with PDT alone showed inflammatory manifestations, while the group treated with GA showed a decrease in vascular proliferation and redness in the dermis. These findings suggest that in psoriasis, GA has a superior anti-inflammatory effect to PDT, which can cause varying degrees of tissue inflammation.

With regard to the PASI scores, all groups except the control group had the highest scores before receiving different drugs. After the administration of different drugs, all groups showed varying degrees of reduction in psoriatic symptoms. However, the group treated with the GA and PDT combination exhibited a better therapeutic effect than the other groups. The scores for erythema, thickening, and scaling were significantly lower (approximately 1) in this group than those in the model group (Fig. 4B−E). The results of *in vivo* potency comparison of blank carrier and free Ce6 with GC NPs/QCS-C NIR are shown in the Supporting Information Fig. S4A and S4B.

The line graph depicting the body weight recordings indicates a continuous downward trend in the body weight of mice during IMQ treatment (Fig. 4F). The spleen, an essential immune organ, reflects the degree of activation of the body's immune system. The spleen/body weight ratio (*w*/*w*) in the model group was approximately 1, which was significantly different from the ratio of approximately 0.3 in the control group. The spleens of mice in the Ce6 NPs/QCS-C and Ce6 NPs/QCS-C NIR groups were also enlarged, possibly due to the inflammatory cascade effect of light damage. In comparison, the spleen/body weight ratio was significantly lower in mice treated with GA, being as low as approximately 0.5 in the GC NPs/QCS-C NIR group (Fig. 4G). This shows that the PDT and GA combination inhibited aberrant immune system activation in psoriatic mice.

To determine the level of inflammation in each mouse group, we measured the serum levels of HMGB1, IL-18, and IL-6 using ELISA kits. The model group showed higher expression levels of HMGB1, IL-18, and IL-6 than the other groups. Furthermore, the group treated with Ce6 NPs/QCS-C NIR showed higher expression levels of HMGB1 and IL-18 than the group treated with Ce6 NPs/QCS-C (Fig. 4H−J). These results indicate that PDT induces accelerated apoptosis in cells while also causing varying degrees of damage to the cells. In the group co-treated with PDT and GA, GA exhibited a significant antagonistic effect on HMGB1, resulting in a reduction in both HMGB1 and IL-18 expression induced by PDT.

3.6. *GC NPs/QCS-C promoted skin tissue repair*

The H&E results indicate that the normal wavy nature of the dermo-epidermal junction was altered in the model group. The same alteration was observed in the Ce6 NPs/QCS-C group. The vascular proliferation in the skin was attenuated in the GA NP group, but no significant improvement in epidermal hyperkeratosis was observed. The groups treated with PDT showed improvement in the epidermal layer thickness, approaching that found in normal mice. However, there was still a noticeable infiltration of mononuclear or multinucleated cells in the dermis (Fig. 5A). Next, we measured the thickness of the stratum corneum in each group of mice. The cuticle thickness reached 70 μm in the model group and decreased to 50 μm under GA or PDT treatment; however, under the GA and PDT combination treatment, the cuticle thickness decreased to 37 μm, which was only about ten micrometers higher than the 25 μm in the control group (Fig. 5B). These findings indicate that the epidermal layer in the group treated with the GA and PDT combination was significantly thin, the epidermis formed a normal wavy edge, and the hypertrophy of the stratum spinosum disappeared.

Skin tissues were analyzed using immunohistochemistry to observe changes in HMGB1 expression at the treatment site (Fig. 5C). All treated groups showed higher expression of HMGB1 mediated by inflammation than in the control group. Its expression was particularly high in the model, Ce6 NPs/QCS-C, and Ce6 NPs/QCS-C NIR groups. In skin tissues, the PDT effect produced by NIR treatment caused cell necrosis and accelerated the apoptosis process. The Ce6 NPs/QCS-C NIR group showed increased HMGB1 expression compared to the Ce6 NPs/QCS-C group, whereas the corresponding GC NPs/QCS-C NIR group showed decreased HMGB1 expression compared to the Ce6 NPs/QCS-C NIR group. The group with the GA and PDT combination exhibited a decrease in HMGB1 expression (Fig. 5D). The expression levels of Ki67, IL-17, and CD3 in the skin tissues were examined using IHC. The model group exhibited high expression levels of Ki67, IL-17, and CD3, while the groups treated with GA NPs, GA NPs/QCS-C, and GC NPs/QCS-C showed decreased expression

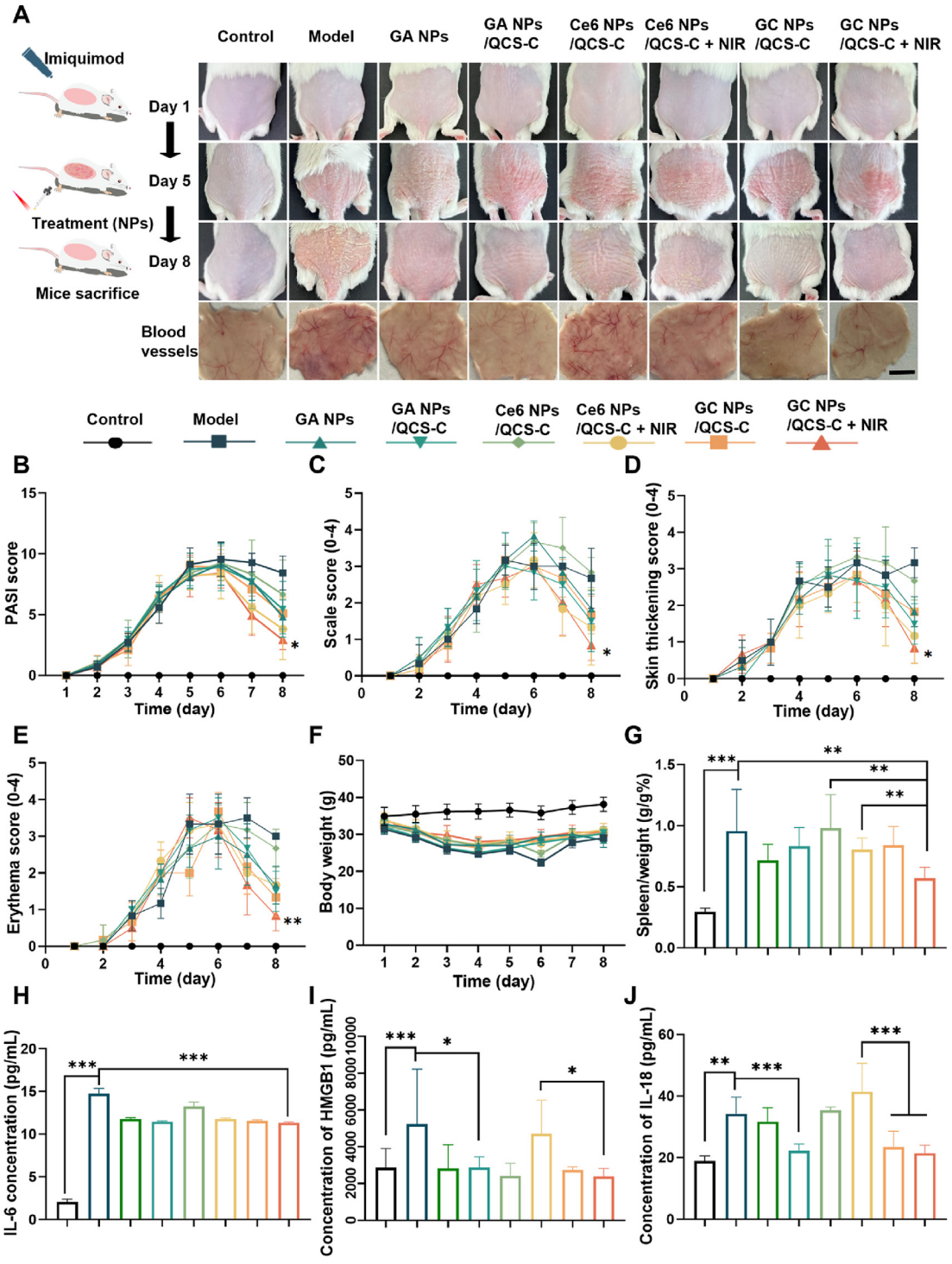

Figure 4 GC NPs/QCS-C ameliorates IMQ-induced psoriasis mice model. (A) Mice dorsal skin characteristics. PASI scores (B), scale scores (C), skin thickening scores (D), erythema scores (E), and body weight (F) of each group during the experimental period were recorded. On Day 8, spleen index (G) levels of IL-6 (H), HMGB1 (I), and IL-18 (J) in serum samples of each group were determined. Data are presented as mean ± SD ($n = 6$). Note: significance as $^{*}P < 0.05$, $^{**}P < 0.01$, $^{***}P < 0.001$.

levels of these factors, possibly due to the anti-inflammatory and immunomodulatory effects of GA. The Ki67 group, which produced PDT under NIR treatment, also exhibited better inhibition of the expression of these factors. These results indicate that co-treatment with GA and NIR significantly reduced the expression levels of Ki67, IL-17, and CD3 (Fig. 5E–G).

3.7. Potential immunoregulatory effects of combination therapy

To gain a better understanding of the immune system changes in psoriasis, we extracted progenitor cells from the spleens of mice (Fig. 6A). The spleens were stained with H&E and showed no significant lesioning effect from the drug (Fig. 6D). We performed

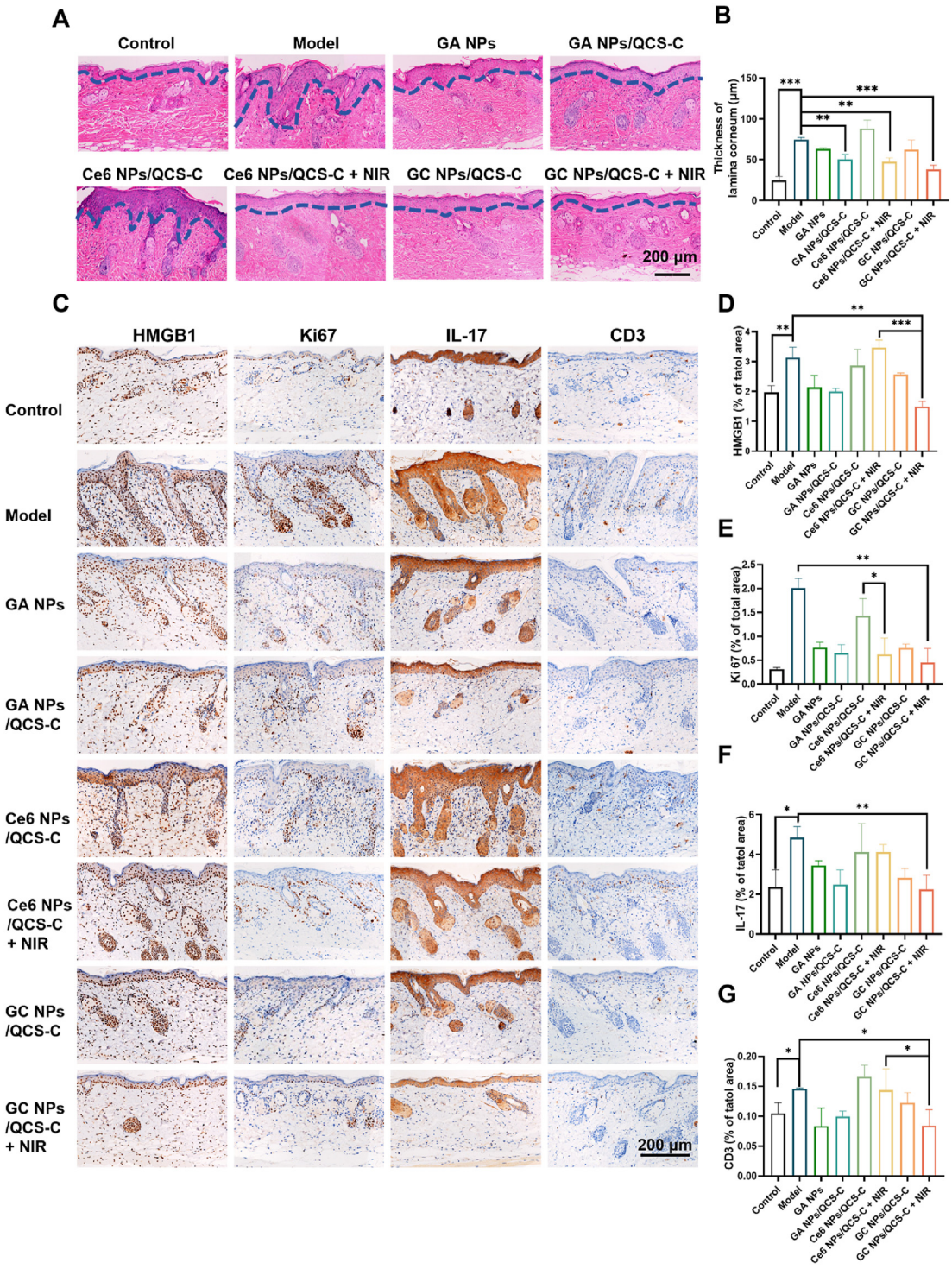

Figure 5 Histopathological analysis of mouse skin. (A) H&E staining analysis. (B) Epidermal thickness in H&E staining analysis. (C) Immunohistochemical staining of HMGB1, Ki67, IL-17, and CD3 antibodies (scale bar = 200 μm). Semiquantitative results of the levels of (D) HMGB1, (E) Ki67, (F) IL-17, and (G) CD3 in each group. Data are presented as mean ± SD ($n = 3$). Note: significance as $^{*}P < 0.05$, $^{**}P < 0.01$, $^{***}P < 0.001$.

FCM analysis of T cells from splenic lymphocytes and used the ratio of T helper/T suppressor cells ($CD4^{+}/CD8^{+}$) as an indicator of immunomodulation[41]. In the IMQ-treated model group, the immune system of mice was abnormally activated, resulting in enlarged spleens and a $CD4^{+}/CD8^{+}$ ratio twice that in normal mice. However, under the GA and PDT combination treatment, the $CD4^{+}/CD8^{+}$ ratio dropped to 3 (Fig. 6B and C).

We also analyzed the changes in MHC-II, CD80, and CD86 in DCs from mouse spleen primary cells using flow cytometry. As expected, the model group showed high expression levels of the maturation markers CD80 (Fig. 7A and B), CD86 (Fig. 7C and D), and MHC-II (Fig. 7E and F) in DCs due to IMQ stimulation[42,43]. However, the combined effect of GA and PDT significantly inhibited the maturation markers in DCs. We then measured the

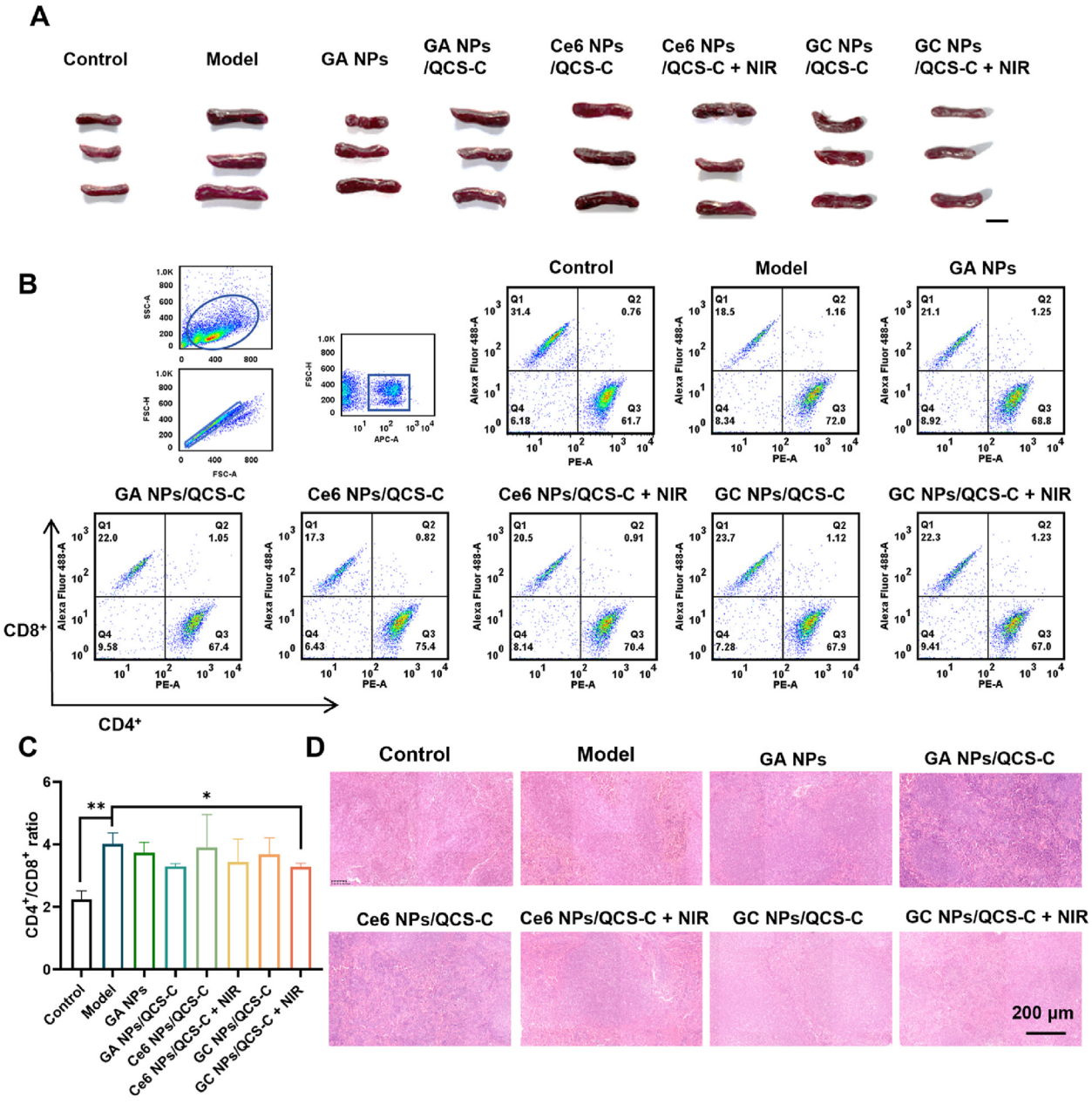

Figure 6 (A) Representative images of spleen organs in each group on Day 8 (scale bar = 1 cm). (B, C) The expression of $CD4^+$ and $CD8^+$ at T cells by FCM analysis. (D) H&E staining of spleen organs in each group (scale bar = 200 μm). Data are presented as mean ± SD ($n = 3$). Note: significance as $^*P < 0.05$, $^{**}P < 0.01$.

levels of MHC-II, CD80, and CD86 on DCs in the dorsal skin of mice in the control, model, and GC NPs/QCS-C NIR groups. The results showed that chemo-photodynamic therapy, both locally and site-specific, inhibited the maturation of DCs, resulting in an anti-psoriatic effect (Supporting Information Fig. S5). These results suggest that the GA and PDT combination is an effective synergistic treatment strategy for psoriasis.

4. Discussion

Although the mechanism of psoriasis is not yet fully understood, abnormal proliferation of human keratinocytes and recruitment of immune cells are known to play vital roles in the onset and progression of psoriasis[44,45]. Similar to tumor cells during their immunogenic death, psoriatic cells release a series of signaling molecules such as HMGB1 and heat shock proteins (HSP70, HSP90) during the injury process. HMGB1 then binds to TLR4, which facilitates the recruitment of immune cells, the maturation of DCs, and the activation of adaptive immune responses. In this study, we utilized the PDT effect produced by the second-generation photosensitizer Ce6 to induce apoptosis of keratinocytes and T cells within the psoriatic lesions and alter the local immune status. The Ce6-induced intracellular ROS production in and apoptosis of the cells confirmed the effects of Ce6 (Fig. 2E and F). The H&E and IHC results demonstrated significant

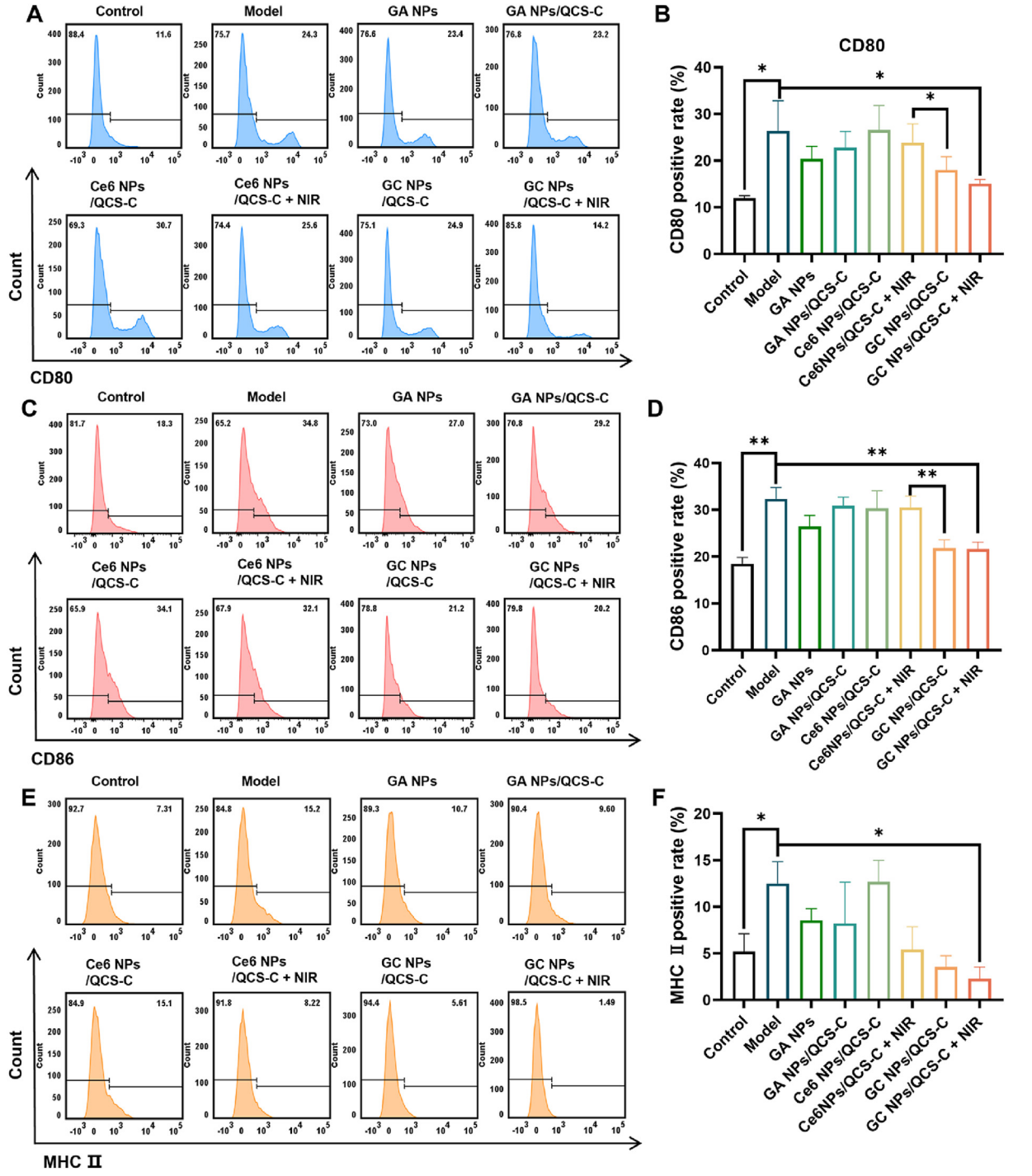

Figure 7 FCM analysis and quantitative results of the expression levels of CD80, CD86, and MHC-II in DC cells from mouse spleen primary cells in each group. Data are presented as mean ± SD ($n = 3$). Note: significance as $^{*}P < 0.05$, $^{**}P < 0.01$.

reductions in the stratum corneum thickness, Ki67 protein level, and T cell infiltration in the skin tissue due to PDT (Fig. 5D and E). However, the application of PDT still faces challenges. The *in vitro* cell experiment results showed that PDT caused significant cell death. The levels of HMGB1 and IL-18 in mice were measured using an ELISA kit. Both HMGB1 and IL-18 exhibited higher expression levels in the Ce6 NPs/QCS-C NIR group than in the Ce6 NPs/QCS-C group (Fig. 4I and J). The IHC results revealed that the lesion sites in the Ce6 NPs/QCS-C NIR group exhibited higher expression levels of HMGB1 and IL-17 than those in the Ce6 NPs/QCS-C group (Fig. 5D and F).

To deliver Ce6, liposomes were formed using GA instead of cholesterol due to the former's amphiphilic nature. This approach addressed the difficulty in drug delivery caused by Ce6's hydrophobicity and promoted the repair of PDT-induced skin damage owing to GA's anti-inflammatory properties. *In vitro* cell

experiments demonstrated that GA-encapsulated Ce6 liposomes did not diminish the ROS production and apoptotic effects of PDT in cells (Fig. 2E and F). *In vivo*, the GA and PDT combination was found to yield more significant therapeutic results than monotherapy. Additionally, GA was found to inhibit the release of HMGB1 due to cell death (Fig. 5D). Thus, these results indicate that the GA and PDT combination is a promising strategy for treating psoriasis with minimal systemic side effects. However, it is important to note that the photodamage and inflammation resulting from PDT can persist. To improve drug efficacy, it is necessary to increase the retention time of the therapeutic agent on the skin. The QCS-C-coated NPs showed superior skin adhesion and penetration ability (Fig. 3A and E), as well as a superior cellular uptake effect, to other NPs, as confirmed by *in vivo* imaging results (Fig. 2A and C).

To compare the therapeutic effects of monotherapy and combination therapy with GA and Ce6, we administered the drugs to mice with IMQ-induced psoriasis. We compared the effects of GA NPs and GA NPs/QCS-C to determine whether QCS-C exacerbated inflammation and prolonged the repair time. The experimental results demonstrated that the GA and PDT combination treatment effectively inhibited abnormal cell proliferation and thereby reduced skin thickness (Fig. 5A and B). Furthermore, mice that received the GA and PDT combination exhibited improved recovery of skin lesions, with decreased expression levels of HMGB1, Ki67, IL-17, and CD3, compared with the model mice (Fig. 5D−G). Additionally, the GA and PDT combination treatment effectively limited the recruitment of immune cells, resulting in a decrease in the $CD4^+/CD8^+$ ratio from 4 to approximately 2 (Fig. 6C). Furthermore, this treatment inhibited expression of the maturation markers CD80, CD86, and MHC-II on splenic DCs (Fig. 7). PDT was unable to effectively address the aberrant activation of the immune system at the psoriatic site. The combination treatment demonstrated a more pronounced maturation inhibitory effect on DCs than monotherapy (Fig. S5), which further highlights the advantage of a multifaceted approach to immune modulation.

5. Conclusions

In sum, considering the potential synergistic benefits of the GA and PDT combination, we fabricated a topical adhesive chemo-photodynamic nanosystem in which GA−lipid framework NPs loaded with Ce6 were coated with QCS-C (GC NPs/QCS-C). Due to their uniform nano-scaled structure, enhanced cellular internalization, and high skin adhesion and penetration, GC NPs/QCS-C could effectively block abnormal epidermal cell proliferation and immune cell infiltration at the lesion site through the potent Ce6-induced PDT effect. As expected, HMGB1 levels were also elevated following PDT, but this elevation was effectively suppressed by GA in the combination treatment. Ultimately, the transdermal administration of GC NPs/QCS-C twice consecutively effectively ameliorated psoriasis-like symptoms, such as skin erythema and squamous and epidermis hyperplasia, in the IMQ-induced psoriasis mouse model and exhibited a high level of biosafety. This formulation effectively suppressed the abnormal overproliferation of skin keratinocytes, reduced the infiltration of inflammatory factors, and normalized immune system activation. This work describes how the GA and PDT combination treatment can address unmet clinical needs in psoriasis and provides a novel chemo-photodynamic combination strategy for psoriasis treatment.

Acknowledgments

This work was supported by funding from the China Postdoctoral Science Foundation (Nos. 2023T160071 and 2021M690488); Natural Science Foundation of Sichuan Province of China for Youths (No. 2023NSFSC1768, China); The Science and Technology Development Fund (SKL-QRCM(UM)2023−2025, China); The State Key Laboratory of Quality Research in Chinese Medicine, University of Macau (No. SKL-QRCM-OP23020, China). The Central Guidance on Local Science and Technology Development Fund of Sichuan (23ZYZYTS0420, China). Multidisciplinary Evaluation of Southwest Characteristic TCM Resources Multidisciplinary Interdisciplinary Innovation Team (No. ZYYCXTD-D-202209, China).

Author contributions

Lijun Su: Writing − original draft, Validation, Software, Investigation. Yixi Zhu: Formal analysis, Data curation. Xuebo Li: Software, Methodology. Di Wang: Resources, Investigation. Xiangyu Chen: Investigation. Zhen Liu: Investigation. Jingjing Li: Methodology, Investigation, Funding acquisition. Chen Zhang: Supervision, Methodology, Funding acquisition. Jinming Zhang: Supervision, Funding acquisition, Conceptualization.

Conflicts of interest

The authors have no conflicts to declare.

Appendix A. Supporting information

Supporting information to this article can be found online at https://doi.org/10.1016/j.apsb.2024.12.020.

References

1. Huang C, Gou KJ, Yue X, Zhao SY, Zeng R, Qu Y, et al. A novel hyaluronic acid-based dissolving microneedle patch loaded with ginsenoside Rg3 liposome for effectively alleviate psoriasis. *Mater Design* 2022;**224**:111363.
2. Wu D, Shou X, Yu YR, Wang XC, Chen GP, Zhao YJ, et al. Biologics-loaded photothermally dissolvable hyaluronic acid microneedle patch for psoriasis treatment. *Adv Funct Mater* 2022;**32**:2205847.
3. Zhou X, Chen YD, Cui L, Shi YL, Guo CY. Advances in the pathogenesis of psoriasis: from keratinocyte perspective. *Cell Death Dis* 2022;**13**:81.
4. Liu HQ, Wang YM, Li WF, Li C, Jiang ZH, Bao J, et al. Anti-psoriasis effects and mechanisms of α-(8-quinolinoxy) zinc phthalocyanine-mediated photodynamic therapy. *Cell Physiol Biochem* 2017;**44**:200−14.
5. Wang YX, Fu SJ, Lu Y, Lai RR, Liu ZY, Luo WX, et al. Chitosan/hyaluronan nanogels co-delivering methotrexate and 5-aminolevulinic acid: a combined chemo-photodynamic therapy for psoriasis. *Carbohydr Polym* 2022;**277**:118819.
6. Nirmal GR, Lin ZC, Lin CH, Sung CT, Liao CC, Fang JY. Polydopamine/IR820 nanoparticles as topical phototheranostics for inhibiting psoriasiform lesions through dual photothermal and photodynamic treatments. *Biomater Sci* 2022;**10**:6172−89.
7. Wang H, Su DD, Huang RF, Shu F, Cheng F, Zheng G. Cellular nanovesicles with bioorthogonal targeting enhance photodynamic/photothermal therapy in psoriasis. *Acta Biomater* 2021;**134**:674−85.
8. Tewari KM, Dondi R, Yaghini E, Pourzand C, Macrobert AJ,

Eggleston IM. Peptide-targeted dendrimeric prodrugs of 5-aminolevulinic acid: a novel approach towards enhanced accumulation of protoporphyrin IX for photodynamic therapy. *Bioorg Chem* 2021;**109**:104667.
9. Wu YH, Li JJ, Zhong XM, Shi JF, Cheng YF, He CL, et al. A pH-sensitive supramolecular nanosystem with chlorin e6 and triptolide co-delivery for chemo-photodynamic combination therapy. *Asian J Pharm Sci* 2022;**17**:206−18.
10. Yu L, Wang ZJ, Mo ZM, Zou BH, Yang YY, Sun R, et al. Synergetic delivery of triptolide and Ce6 with light-activatable liposomes for efficient hepatocellular carcinoma therapy. *Acta Pharm Sin B* 2021;**11**: 2004−15.
11. Liu YB, Chen XC, Yu BX, Cen Y, Huang CY, Yan MY, et al. Chimeric peptide-engineered self-delivery nanomedicine for photodynamic-triggered breast cancer immunotherapy by macrophage polarization. *Small* 2023;**20**:2309994.
12. Liu ZY, Wu XP, Dai K, Li RK, Zhang JM, Sheng DK, et al. The new andrographolide derivative AGS-30 induces apoptosis in human colon cancer cells by activating a ROS-dependent JNK signalling pathway. *Phytomedicine* 2022;**94**:153824.
13. Yang J, Liu XJ, Cao YJ, Wang PR, Zhang HY, Chen Q, et al. 5-Aminolevulinic acid photodynamic therapy *versus* minocycline for moderate-to-severe rosacea: a singlecenter, randomized, evaluator-blind controlled study. *J Am Acad Dermatol* 2023;**89**: 711−8.
14. Zhang WG, Guo S, Li B, Liu L, Ge R, Cao TY, et al. Proinflammatory effect of high-mobility group protein B1 on keratinocytes: an autocrine mechanism underlying psoriasis development. *J Pathol* 2016; **241**:392−404.
15. Jin LL, Zhu ZX, Hong LJ, Qian ZF, Wang F, Mao ZW. ROS-responsive 18β-glycyrrhetic acid-conjugated polymeric nanoparticles mediate neuroprotection in ischemic stroke through HMGB1 inhibition and microglia polarization regulation. *Bioact Mater* 2023;**19**: 38−49.
16. Chen T, Fu LX, Guo ZP, Yin B, Cao N, Qin S. Involvement of high mobility group box-1 in imiquimod-induced psoriasis-like mice model. *J Dermatol* 2016;**44**:573−81.
17. Yamaguchi H, Kidachi Y, Kamiie K, Noshita T, Umetsu H. Structural insight into the ligand-receptor interaction between glycyrrhetinic acid (GA) and the high-mobility group protein B1 (HMGB1)-DNA complex. *Bioinformation* 2012;**8**:1147−53.
18. Chen D, Bellussi LM, Cocca S, Wang J, Passali GC, Hao X, et al. Glycyrrhetinic acid suppressed hmgb1 release by up-regulation of Sirt6 in nasal inflammation. *J Biol Regul Homeost Agents* 2017;**31**: 269−77.
19. Shi XD, Yu LJ, Zhang YL, Liu ZQ, Zhang HW, Zhang YS, et al. Glycyrrhetinic acid alleviates hepatic inflammation injury in viral hepatitis disease *via* a HMGB1-TLR4 signaling pathway. *Int Immunopharmacol* 2020;**84**:106578.
20. Lu QR, Han WT, Wen DF, Guo P, Liu Y, Wu ZY, et al. 18β-Glycyrrhetinic acid alleviates *P. multocida*-induced vascular endothelial inflammation by PARP1-mediated NF-κB and HMGB1 signalling suppression in PIEC Cells. *Infect Drug Resist* 2023;**16**: 4201−12.
21. Czarnowicki T, He H, Leonard A, Kim HJ, Kameyama N, Pavel AB, et al. Blood endotyping distinguishes the profile of vitiligo from that of other inflammatory and autoimmune skin diseases. *J Allergy Clin Immunol* 2019;**143**:2095−107.
22. Chen YC, Yan YH, Liu H, Z Qiu FF, Liang CL, Zhang QF, et al. Dihydroartemisinin ameliorates psoriatic skin inflammation and its relapse by diminishing $CD8^+$ T-cell memory in wild-type and humanized mice. *Theranostics* 2020;**10**:10466−82.
23. Lee WH, Rho JG, Yang Y, Lee S, Kweon S, Kim HM, et al. Hyaluronic acid nanoparticles as a topical agent for treating psoriasis. *ACS Nano* 2022;**16**:20057−74.
24. Hazari AS, Kaur H, Karwasra R, Abourehab MAS, Khan AA, Kesharwani P. An overview of topical lipid-based and polymer-based nanocarriers for treatment of psoriasis. *Int J Pharm* 2023;**638**:122938.
25. Rachamalla HK, Voshavar C, Arjunan P, Mahalingam G, Chowath RP, Banerjee R, et al. Skin-permeable nano-lithocholic lipidoid efficiently alleviates psoriasis-like chronic skin inflammations. *ACS Appl Mater Inter* 2022;**14**:14859−70.
26. Pukale SS, Sharma S, Dalela M, Singh Ak, Mohanty S, Mittal A, et al. Multi-component clobetasol-loaded monolithic lipid-polymer hybrid nanoparticles ameliorate imiquimod-induced psoriasis-like skin inflammation in Swiss albino mice. *Acta Biomater* 2020;**115**:393−409.
27. Xu ZY, Huang Y, Wu YH, Chen JM, Seto SW, Leung GPH, et al. Glycyrrhizic acid-lipid framework nanovehicle loading triptolide for combined immunochemotherapy. *ACS Appl Mater Inter* 2023;**15**: 41337−50.
28. Iqbal Y, Ahmed I, Irfan MF, Chatha SAS, Zubair M, Ullah A. Recent advances in chitosan-based materials; the synthesis, modifications and biomedical applications. *Carbohydr Polym* 2023;**321**:121318.
29. Wang H, Wang CP, Zou Y, Hu JJ, Li YW, Cheng YY. Natural polyphenols in drug delivery systems: Current status and future challenges. *Giant* 2020;**3**:100022.
30. Chen WL, Yuan ZQ, Liu Y, Yang SD, Zhang CG, Li JZ, et al. Liposomes coated with *N*-trimethyl chitosan to improve the absorption of harmine *in vivo* and *in vitro*. *Int J Nanomedicine* 2016;**11**:325−36.
31. Xian J, Zhong XM, Gu H, Wang X, Li JX, Li JJ, et al. Colonic delivery of celastrol-loaded layer-by-layer liposomes with pectin/-trimethylated chitosan coating to enhance its anti-ulcerative colitis effects. *Pharmaceutics* 2021;**13**:2005.
32. Fereig SA, El-Zaafarany GM, Arafa MG, Abdel-Mottaleb MMA. Tacrolimus-loaded chitosan nanoparticles for enhanced skin deposition and management of plaque psoriasis. *Carbohydr Polym* 2021;**268**: 118238.
33. Luesakul U, Puthong S, Sansanaphongpricha K, Muangsin N. Quaternized chitosan-coated nanoemulsions: a novel platform for improving the stability, anti-inflammatory, anti-cancer and transdermal properties of Plai extract. *Carbohydr Polym* 2020;**230**:115625.
34. Wei Z, Gao Y. Evaluation of structural and functional properties of chitosan-chlorogenic acid complexes. *Int J Biol Macromol* 2016;**86**: 376−82.
35. Rui YL, Xie MH, Hu B, Zhou L, Saeeduddin M, Zeng XX. Enhanced solubility and antioxidant activity of chlorogenic acid-chitosan conjugates due to the conjugation of chitosan with chlorogenic acid. *Carbohydr Polym* 2017;**170**:206−16.
36. Li FJ, Yan YY, Gu CZ, Sun JY, Han YR, Huangfu ZQ, et al. Preparation and characterization of phenolic acid-chitosan derivatives as an edible coating for enhanced preservation of saimaiti apricots. *Foods* 2022;**11**:3548.
37. Duan Y, Jiang FC, Li Q, McDowell A, Li YX, Wang Y, et al. Multifunctional polysaccharide/metal/polyphenol double-crosslinked hydrogel for infected wound. *Carbohydr Polym* 2024; **332**:121912.
38. Xian J, Zhong XM, Huang Q, Gu H, Feng YX, Sun JY, et al. N-Trimethylated chitosan coating white adipose tissue vascular-targeting oral nano-system for the enhanced anti-obesity effects of celastrol. *Int J Biol Macromol* 2023;**236**:124023.
39. Yue X, Zhao SY, Qiu MY, Zhang JB, Zhong GF, Huang C, et al. Physical dual-network photothermal antibacterial multifunctional hydrogel adhesive for wound healing of drug-resistant bacterial infections synthesized from natural polysaccharides. *Carbohydr Polym* 2023;**312**:120831.
40. Zhou JJ, Lin ZX, Ju Y, Rahim MA, Richardson JJ, Caruso F. Polyphenol-mediated assembly for particle engineering. *Acc Chem Res* 2020;**53**:1269−78.
41. Rudolphi A, Spie S, Conradt P, Classon MH, Reimann J. $CD3^+$ T cells in severe combined immune deficiency (scid) mice. I. Transferred

purified $CD4^+$ T cells, but not $CD8^+$ T cells are engrafted in the spleen of congenic scid mice. *Eur J Immunol* 1991;**21**:523−33.
42. Hirano H, Yoshioka T, Yunoue S, Fujio S, Yonezawa H, Niiro T, et al. TLR4, IL-6, IL-18, MyD88 and HMGB1 are highly expressed in intracranial inflammatory lesions and the IgG4/IgG ratio correlates with TLR4 and IL-6. *Neuropathology* 2012;**32**:628−37.
43. Xi L, Lin ZB, Qiu F, Chen SK, Li P, Chen X, et al. Enhanced uptake and anti-maturation effect of celastrol-loaded mannosylated liposomes on dendritic cells for psoriasis treatment. *Acta Pharm Sin B* 2021;**12**:339−52.
44. Gangadevi V, Thatikonda S, Pooladanda V, Devabattula G, Godugu C. Selenium nanoparticles produce a beneficial effect in psoriasis by reducing epidermal hyperproliferation and inflammation. *J Nanobiotechnology* 2021;**19**:101.
45. Gomez C, Muangnoi C, Sorasitthiyanukarn FN, Wongpiyabovorn J, Rojsitthisak P, Rojsitthisak P. Synergistic effects of photo-irradiation and curcumin-chitosan/alginate nanoparticles on tumor necrosis factor-alpha-induced psoriasis-like proliferation of keratinocytes. *Molecules* 2019;**24**:1388.